SPECIMEN CLAMPING AND PERFORMANCE OF THE IOISIPESCU SHEAR TESTS APPLIED FOR COMPOSITE MATERIALS

Jonas M. Neumeister, L. Niklas Melin
Solid Mechanics, KTH - Royal Institute of Technolog, SE -100 44 Stockholm, Sweden

Keywords: *Iosipescu Shear Composite Clamping Numerical Experiment Verification*

Abstract

*Clamping and subsequent loading in shear of Ioispescu specimens is investigated. Combined stresses reach similar, or even higher, levels locally compared the nominal shear stress, both compressive and tensile. Especially for brittle materials, composites, and materials with anisotropic failure modes, these stresses may cause premature failure outside the test region and appropriate clamping levels become important. A clamping ratio (*r*) between clamping force and peak shear force is introduced, and it is shown that for quasi-isotropic failure modes, the overall lowest detrimental stresses are obtained for about* r *~1. It is further shown that loss of contact always occurs in one part of the clamping region unless* r *is in excess of 2.5-3. Near that loss of contact, high tensile stresses are obtained. Even with moderate* r*, there will be local plasticity or crushing etc due to high contact pressure near the end of the opposing gripping face. These findings are shown both numerically and experimentally using optical full field strain measurements.*

1 Introduction and Background

When testing for shear properties of isotropic (e.g. ductile metallic) materials, the Iosipescu test is well suited. Clamping, minor imperfections, even fixture function are no major issues for test performance. This is quite different when it comes composites: material orthotropy, both elastic and regarding strength properties, as well as failure initiation and –modes, and evolving damage severely influence test performance[1-3].

Using a quite simple rescaling technique, a modified Ioispecu specimen geometry efficiently eliminates the effects of elastic orthotropy and renders very uniform stress- and strain profiles[3,4]. This facilitates testing for strengths and constitutive properties up to much higher levels. Then also proper clamping and other issues which may cause premature failure become more important. Fibrous composites, especially those with one dominating direction are particularly sensitive to crushing in the clamped region, and stresses there arise from both clamping pressure and subsequently from the increasing nominal shear load. Furthermore, such materials are often sensitive also to transverse tensile stresses, which arise near the clamped area, but on the opposite face of the high contact pressures.

No general recommendations for clamping levels exist, but both too firm and too loose clamping is detrimental, often for either one of the two reasons mentioned above. Generally, adequate clamping forces should scale with the (expected) maximum transferred shear force in a test. The purpose of the present study is to establish proper clamping force levels for Iosipescu shear test when using composite specimens, and give guidelines how to handle the widely varying properties of each such material individually.

2 Analysis: Notation and Clamping Model

Combined stresses are at its highest, and presumably most damaging level as the highest transferred shear load is approached near the end of a test. Thus, the notation of a clamping ratio r, the ratio between clamping force and highest net shear load, is introduced as

$$r = P_{cl} / \hat{P}_{sh} \tag{1}$$

and is henceforth used to characterize a certain clamping level. Although nonlinearities in material behaviour, degradation and contact conditions will influence the results even when r is kept constant among different tests, such effects will be disregarded at this stage. Here, the purpose is to give quite general guidelines regarding suitable clamping ratio r and how to address such issues.

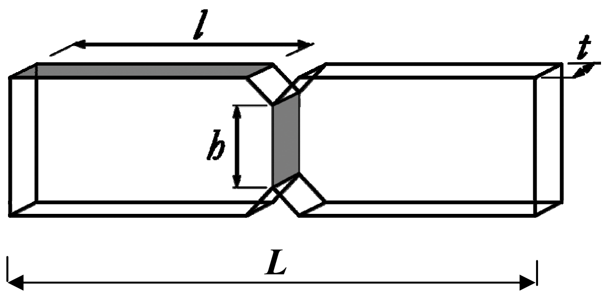

Fig. 1. The Iosipescu specimen and typical measures

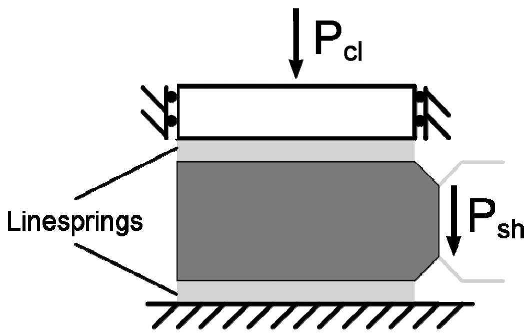

Fig. 2. Schematic of the fixture, clamping, half a specimen, application of loadsets, used in the model

Referring to the dimensions shown in Fig. 1, the clamping force P_{cl} of Eq. 1 is the resultant of the average clamping pressure $\bar{p}_{cl}$ as

$$P_{cl} = \bar{p}_{cl} \cdot l \cdot t, \qquad (2)$$

whereas the highest net shear load $\hat{P}_{sh}$, is related to the (anticipated) peak shear stress $\hat{\tau}$ in the specimen through

$$\hat{P}_{sh} = \hat{\tau} \cdot h \cdot t. \qquad (3)$$

Each of these two loads will result in normal stresses in the clamping region. The shear load tends to both displace and tilt the clamped part of the specimen (see Fig. 2), and using a simple line-spring model for its support gives maximum stress levels of

$$\pm \hat{p}_{sh} = \frac{\hat{\tau}}{2}\left[1 + 3 \cdot \left(\frac{L}{l} - 1\right)\right]\frac{h}{l}. \qquad (4)$$

The first term inside the square brackets refers to the translation of the clamped half of the specimen, and the second to its tilt. Stresses arise on both top and bottom faces and are of opposite sign, and their combined resultants balance the transferred shear through the test region net section. (These stress distributions are equivalent to the ones arising in a column of cross section $t \times h$, loaded eccentrically by $\hat{P}_{sh}/2$ in compression or tension respectively, cf. Fig. 2) Their highest levels are encountered at the end closest to the test region, compressive on the bottom side and tensile on top.

During testing, these stresses are superimposed on the pre-existing clamping pressure $\bar{p}_{cl}$, and peak levels of the combined contact stresses are the potentially damaging ones (from Eqs. 2 and 4)

$$\hat{p}_{tot} = \bar{p}_{cl} + \hat{p}_{sh} = \frac{P_{cl}}{l \cdot t} + \frac{\hat{\tau}}{2}\left(3 \cdot \frac{L}{l} - 2\right)\frac{h}{l}. \qquad (5)$$

Failure levels for both $\hat{\tau}$ and $\hat{p}$ are of course related and depend the specific material used. However, one convenient (and not completely unreasonable, but probably conservative) estimate would be through the von Mises effective stress, so that peak admissible contact pressure relates to the shear strength as

$$\hat{p} = \sqrt{3} \cdot \hat{\tau}. \qquad (6)$$

With Eqs. 5 and 6, an upper limit to the suitable clamping ratio can be established (after some rearrangement)

$$r = \frac{P_{cl}}{\hat{P}_{sh}} \leq \sqrt{3}\frac{l}{h} - \frac{3 \cdot L}{2 \cdot l} + 1, \qquad (7)$$

which gives (with typically h = 12, l = 34, and L = 80 [mm]) that in order to avoid widespread irreversible compressive deformation, a reasonable limit on the clamping ratio should be $r \leq 2.37$. Likewise, requiring that this fairly simple model outlined above maintains a positive contact pressure over the entire grip length, i.e. that $\bar{p}_{cl} - \hat{p}_{sh} \geq 0$ everywhere gives a lower limit of

$$r = \frac{P_{cl}}{\hat{P}_{sh}} \geq \frac{3 \cdot L}{2 \cdot l} - 1, \qquad (8)$$

implying that $r \geq 2.53$ for the same geometry.

Thus, even with the quite simplistic model outlined here, it is seen from Eqs. 7 and 8 that two conflicting requirements exist which cannot be met simultaneously: i)gripping without loss of contact throughout the entire test, and ii)avoiding irreversible deformation or damage in significant parts of the clamped region.

So far, no reference has been made to the actual material tested (apart from Eq. 6). In a ductile isotropic material, neither partial loss of contact or local plasticity due to locally high contact pressure will be particularly detrimental to test performance. However, for brittle materials, and composites more sensitive to certain types of loads or directions, these issues are highly relevant.

It may be noted that higher compressive strengths than stated by Eq. 6 (which may very well be the case for fiber composites) suggest higher admissible clamping ratios r. Moreover, clamping ratios in the range of $r \geq 2.5$ are deemed to be very high compared to common experimental practice. This implies two things: on the gripping face which is unloaded through applying the nominal shear load, loss of contact will very likely occur, and secondly and as a consequence, as contact is lost there, the contact pressure on the opposite gripping face will increase even further, i.e. to even higher levels than stated by Eq. 5.

One other issue is that many composite materials exhibit anisotropic, most often orthotropic elastic behaviour, and consequently that stress results for given boundary conditions and loads may differ substantially among different materials. Encouragingly enough however, very even and almost identical stress distributions due to the nominal load can be accomplished in materials with a wide range of degrees of orthotropy. This is achieved through rescaling the specimen geometry, specifically the notch opening angle 2θ [3,4], according to

$$2\theta = 2 \cdot \arctan\left(\frac{\tan 55^\circ}{\sqrt[4]{\lambda}}\right) \qquad (9)$$

wherein 55° comes from half the optimal notch opening angle for an isotropic material (110°), and λ is the degree of material orthotropy defined as

$$\lambda = \frac{E_y}{E_x}. \qquad (10)$$

Note that Eqs. 9 and 10 prescribe different notch opening angles for the same material depending on its orientation vs. the specimen. Generally, testing is easier and results are better for the stronger material direction oriented along the x-axis, i.e the stronger direction oriented across the test region. Usually this is also the stiffer direction, the direction with the largest fiber content, which implies that wider angle is appropriate, i.e. that $2\theta \geq 110^\circ$, see [3, 6].

Superimposed on the stresses arising from the nominal shear loading are the clamping stresses. These however, are very uniform in the gripping region, especially if the transition from gripping to non-gripping is benign as it should through a rounded and small angle. In any case, gripping stresses alone depend primarily on clamping force and not on material properties.

It should be noted that all stresses mentioned have been calculated using linear elasticity and also approximate models. Stresses from both the line spring type clamping and the orthotropic rescaling are approximate. However, those effects are of minor importance since their relevant effects are of similar magnitude as is experimental precision and repeatability [3,6].

Moreover, the materials at hand are rarely linearly elastic up to peak stresses. Rather significant non-linearities and irreversible strains, degradation, damage etc, arise during a test whose purpose most often is to test exactly such behaviour. Concurrently, other nonlinear effects develop during a test: such may be sliding, friction, loss of contact, dependence on loading history etc. All those non-linear effects combined impede truly universal or general statements to be made regarding how stresses evolve while clamping and testing of materials. However, some generalisations are still possible. These will be addressed next.

3 Non-linearities and Stress Field Interpretation

The definition of a clamping ratio r (as in Eq. 1) describes actual specimen gripping in reference to the anticipated test, i.e. expected peak stress levels. However, in a general experimental situation material behavior at all load levels up to peak is of interest, and stress states in both test- and gripping regions change continuously. It is thus expedient to define also a current clamping ratio r_c analogously to Eq. 1, but with the current shear force P_{sh} instead of its expected peak value. Hence, during a test the current clamping ratio r_c starts at infinity (no net shear applied) and decreases towards the final value, the clamping ratio r for the actual test.

If conditions were isotropic, linearly elastic and if kinematic boundary conditions were constant, strict proportionality would apply and superposition of the two loadsets (clamping and shear) and thus their resulting stress fields would be possible. (Strictly, also Poisson's ratio ν must be kept constant, but in reality ν is if minute significance). Then, all stresses would be unambiguously determined by the given r_c, apart from a scaling to the appropriate load level.

With a material, of general orthotropic elastic properties (even with rescaled notch angle), these superposition- and scaling features become invalid (in the strict sense). However, the introduced inaccuracies are quite small and of similar magnitude as the ones resulting from non-linear boundary conditions (as will be shown below). And compared to the material non linear behavior arising at higher loads, which certainly may differ immensely among different composites, these effects are even smaller.

The question at hand is how well do the stress fields for a given clamping ratio r_c, but at different load magnitudes, compare to each other (when scaled properly)? If these differences are notably smaller than other sources of error (damage, degradation, considerable material non-linearity, experimental scatter), then for practical purposes stress fields throughout the entire test, i.e. for any r_c. may be well approximated with the ones calculated at peak stress levels for a particular clamping ratio r. And further that these calculations are fairly insensitive to elastic properties and strengths.

It has been shown[7] that for an isotropic materials the relevant parameter is $\hat{\tau}/E$ (or $\hat{\tau}/G$), and that testing one material at a different lower load level τ (at a certain fraction of $\hat{\tau}$) is equivalent to testing another material which is stiffer by the same fraction (i.e. whose E and G are higher) at stress level $\hat{\tau}$. In other words, that at a given r_c, lower absolute loads are equivalent to higher material stiffnesses by the same factor, and stresses only differ through that scaling factor.

Conversely, this means that by interpreting calculated stress fields for a given r (at load level $\hat{\tau}$) as also representative for stress fields, at current clamping ratio $r_c = r$ (but at lower net shear load τ), produces the same inaccuracies as using a erroneous Young's modulus at $\hat{\tau}$. And consequently, if the differences among stress fields calculated for quite widely varying moduli are minor, essentially the same stresses can be expected at other loads (but for the same r_c-value) if properly rescaled.

4 Numerical Model: Clamping and Loading

Using the commercial FE-code ABAQUS version 6.6, the clamping and subsequent loading were modeled numerically for specimens of perfect geometry (cf. Fig. 1). Standard elements of hex-type with 8 nodes and reduced integration were used. Clamping between four rigid planes simulated the fixture. Both clamping- and shear loads were applied to those planes. Contact between fixture and specimen was defined and normal separation was allowed for where such was anticipated. Tangential sliding was allowed for through a penalty formulation and with a coefficient of friction μ, which was assumed to be between 0.4 and 0.8.

As mentioned above, and demonstrated further on, detailed stress fields are fairly insensitive to elastic moduli why a 'neutral' material was modeled here. Thus, isotropic material behavior was assumed with modulus E = 70 GPa and Poisson's ratio of ν = 0.3 (representative for e.g. aluminum). To asses an appropriate peak loading level, a shear strength of $\hat{\tau}$ = 150 MPa was chosen (corresponding to yield stress of σ_s = 260 MPa, see Eq. 6). Accordingly, numerical results will be strictly valid for all materials with a ratio of $\hat{\tau}/E = 0.21\%$. For most composites that value would be similar or higher since elastic moduli, especially in the preferred (compliant) clamping direction, tend do be lower.

Notch opening angle ($2\theta = 110°$) and specimen geometry were chosen as stated in Section 2. The loading sequence involved first a clamping force applied up to the predetermined clamping ratio r, followed by subsequent increase of shear load up to levels corresponding to $\hat{\tau}$. Since nominal loading involved non-linear effects of contact, friction and separation, this monotonic increase took place in loads steps to ensure convergence of solution.

The investigated clamping ratios ranged from r = 0 to 5.9, in 13 steps, and the highest r corresponds to a contact pressure of 1.2 times the yield stress (although only elastically modelled). Such a large interval was chosen since stress fields at high r may be interpreted as (merely scaled) versions of stress fields at intermediate test stages, i.e. at $r_c \geq r$, where high r_c correspond to early test stages.

5 Numerical Results: Clamping and Loading

The simple model in Section 2 gives a constant clamping pressure $\bar{p}_{cl}$, and also numerically quite even clamping stresses were obtained (apart from at the very ends of those regions). Upon increasing shear load (i.e. as r_c decreases towards r) and considering the left specimen half (see Figs. 1 and 2), the upper gripping face is unloaded, the lower one experiences higher net forces, and simultaneously the gripped specimen part wants to rotate due to the bending applied through pure shear in the specimen center. Hence, these effects, i.e. increasing contact pressure (lower face) and decreasing pressure (upper face), are the most pronounced in the part of the clamped regions closest to the test region. (see Fig. 2)

a)

b)

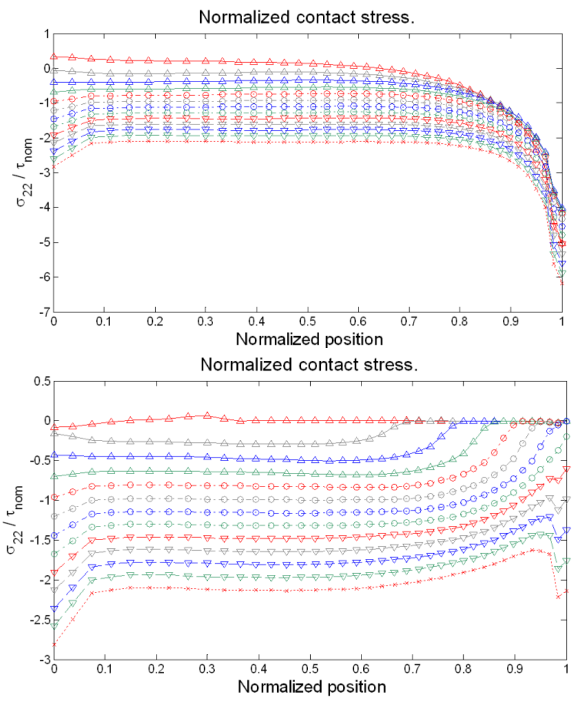

Fig. 3. Normalized contact stresses on: a) lower clamping surface and b) upper face. Clamping ratio $r \in [0 \ldots 5.9]$ in 13 steps of ~0.5 from top to bottom

In Figs. 3ab, the (normalized) contact pressures are shown for the upper and lower clamping faces can be seen for 13 steps of $r \in [0 \ldots 5.9]$. It is clearly seen that shear loading always produces very high contact pressures near the end of the lower clamping face, and that clamping pressure elsewhere remains rather constant. On the upper face, however, it is seen that loss of contact may occur over up to one third of the clamping face (for moderate r), and that very high clamping ($r > 3$) is required to completely avoid this.

In Figs. 4ab, the position of loss of contact, and the highest (calculated) contact pressure are shown (normalized) as a function of claming ratio r (and thus also current r_c). For the latter, there seems to be an optimal clamping ratio of r ~ 1, which minimizes peak pressure, although still large (about four times τ). Note however, that stresses are singular near that corner and that this value depends on FE mesh size.

a) b)

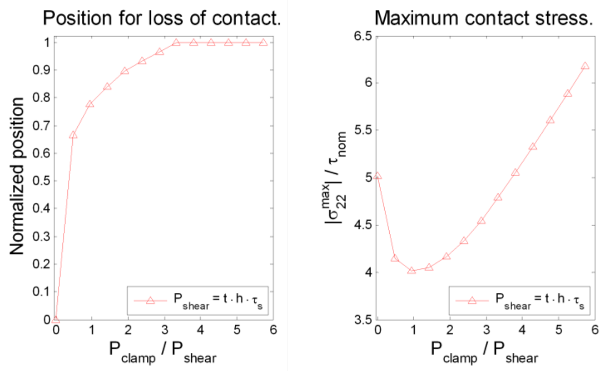

Fig. 4. Dependence on clamping ratio r: a) position for loss of contact (on upper face) , and b) peak contact pressure (at edge of lower face)

Under the clamping face with receding contact as τ is increased, tensile stresses arise, which is clearly seen in Fig. 5. These are in the order of, but slightly higher, than the nominal shear stress τ for low to moderate r. Their (normalized) peak level is plotted versus r in Fig. 6, and interestingly a peak of ~1.35 τ appears for r = 1.5. However, they are only slightly lower for higher or lower (but still reasonable) r- values.

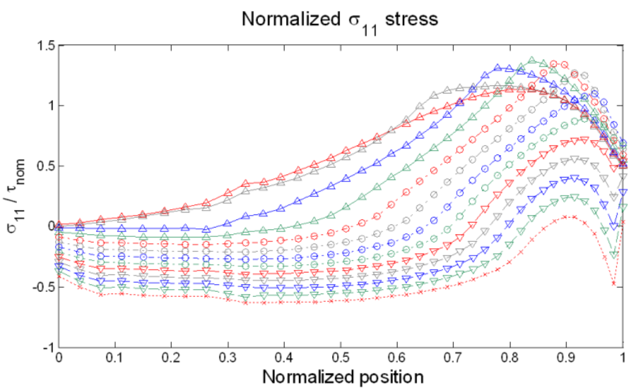

Fig. 5. Profiles of tensile stress along the upper clamping surface. Clamping ratio $r \in [0 \ldots 5.9]$ in 13 steps of ~0.5 from top to bottom

Finally, in Figs. 7ab it is demonstrated that all normalized stress profiles from Figs. 3 and 5 may readily be interpreted not only at $\hat{\tau}$ and r, but also for each intermediate lower τ (and an accordingly higher r_c). There, three stress profiles each are shown for lower and upper clamping face respectively, evaluated at r = 1, but also calculated for Youngs moduli changed to five times and one fifth of the original value.

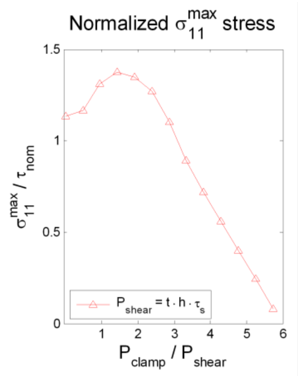

Fig. 6. Peak tensile stress versus clamping ratio r

a)

b)

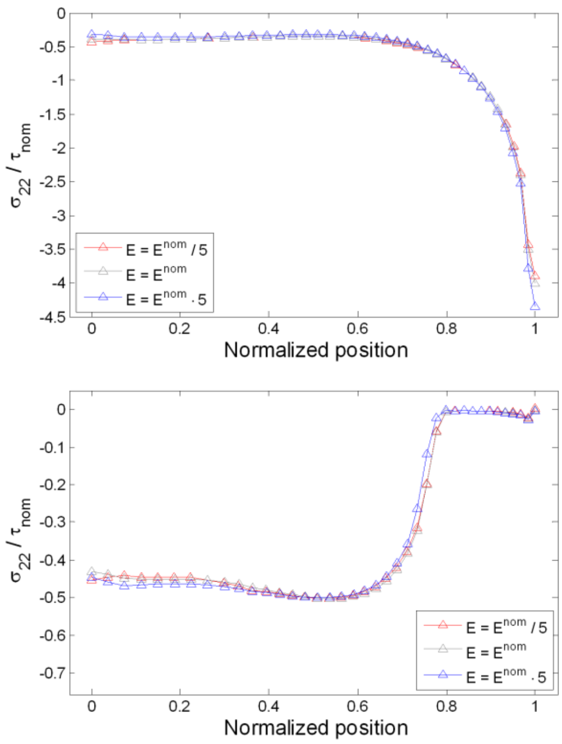

Fig. 7. Dependence on variation of Young's modulus E by a factor of five (up or down) for contact pressures on a) lower face, and b) upper face. Both at r = 1

Obviously, the different stress profiles are hardly distinguishable, and they are, as described in Section 3, equivalent to changing the load levels by a factor of five (up or down), and consequently as valid as if r_c is varied by a factor of 25. Similar calculations show that there is essentially no dependence on the coefficient of friction.

6 Experimental and Verification

For the purpose of good strain resolution for the optical whole field measurements, a quite compliant PMMA material (plexiglass) was used for the specimens in the experiments. More details about the Digital Speckle Photography (DSP-) measurements and the in-house built improved Ioispescu fixture are available in references [3, 6].

With a youngs modulus of E_{PMMA}= 2.7 GPa, shear modulus G_{PMMA}= 1.0 GPa, and a tensile strength ~70 MPa and thus estimated $\hat{\tau}$ of ~40 MPa, the material characterization ratio becomes $\hat{\tau} / E = 1.4\%$ which distinctly higher than for many metals, and comparable to values for some high performance composite. The specimen was clamped to a measured strain of $\varepsilon_{cl} = -0.367$ MPa, which corresponds to approximately $\bar{p}_{cl}$ = 10 MPa, and subsequently loaded in steps up to τ = 25 MPa, giving a final clamping ratio of about r = 1.1 (cf. Eqs. 1-3).

Strain fields where recorded for each load step and the two normal strain components can be seen in Figs. 8ab at the highest load for the clamped left half of the specimen.

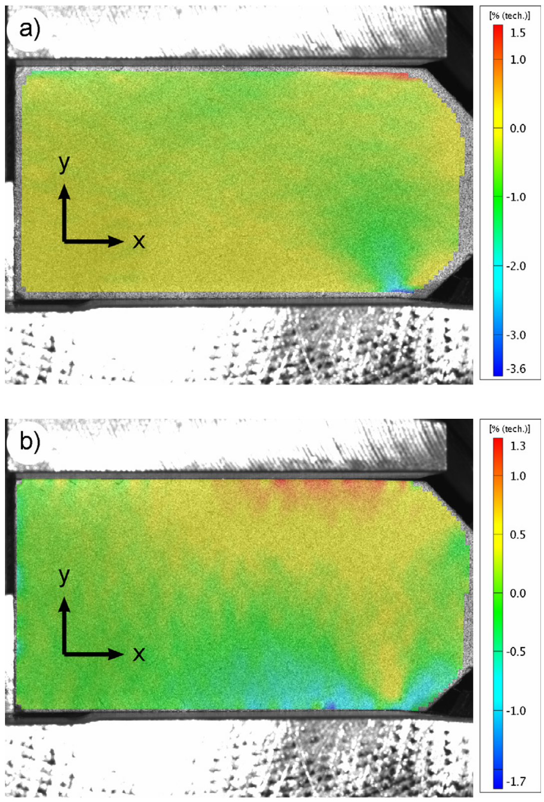

Fig. 8. Experimentally observed normal strain fields: a) clamping (ε_y) and b) lengthwise (ε_x)

Strains were evaluated along the top and bottom clamping surfaces, but within the specimen. Such strain profiles are shown in Fig. 9ab. As loss of contact was anticipated along the top surface, optical facets covering also the edge of the clamping device were there included in the strain calculations. As surface separation progressed, this was seen as large (positive) tensile strains, cf. Fig. 9b. These are however not true material strains. Instead they show how the point of loss of contact moves inward into the gripping section (and they also indicate the amount of separation). As a consequence of this evaluation procedure, also strains in the gripping section are somewhat underestimated.

a)

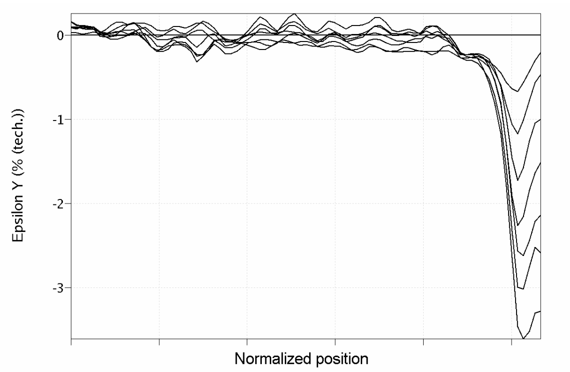

b)

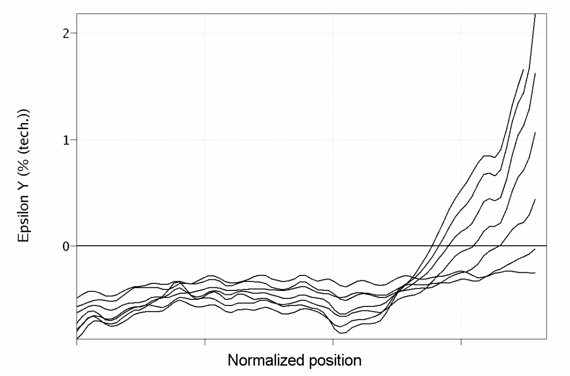

Fig. 9. Clamping strain (ε_y) profiles along for increasing loads (up to r ~1.1): a) bottom face, and b) top surface. Note: the high and (artificial) positive strain values on the top face are calculated over the separating faces at loss of contact

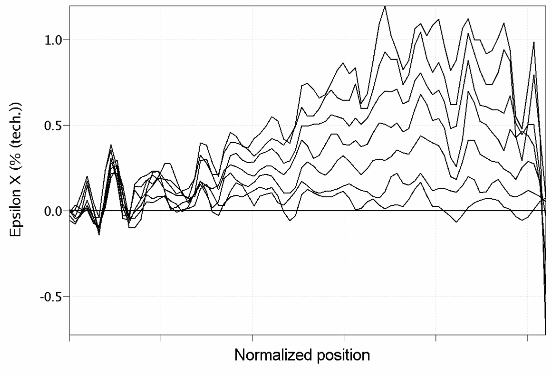

Fig. 10. Tensile strain profiles of ε_x (lengthwise) along the upper clamping surface where loss of contact occurs.

In Fig. 10, finally, profiles of the tensile strain ε_x (from Fig. 8b) along the specimen top surface are shown for increasing shear load.

Although the calculated stresses (apart from τ which is measured) and optically measured strains presented in this section should be regarded as indicative and/or subject to experimental scatter, it is quite instructive to study their magnitudes. The clamping pressure $\bar{p}_{cl}$ is calculated from average strains in the entire gripping section (assuming a uniaxial state of stress), which gives a clamping ratio close to the targeted r ~1. Shear strains in the test region at τ = 25 MPa are in the order of γ = 2.4%. Peak compressive strains on the bottom face are about -3.6% which (elastically) corresponds to about σ_y = -97 MPa (presumably above the linear range of PMMA). Highest tensile strains along the top face reach about ε_x = 1.1%, which corresponds to roughly σ_x = 30 MPa.

Another noteworthy observation is how the loss of contact evolves already at low loads, it can here be seen (Fig. 9b) to occur between the first and second loadstep (corresponding to r_c between 5 and 3). At subsequent higher shear loads, the point of separation moves inwards and at r ~ 1.1, roughly 20% of the upper gripping surface have separated.

All these estimates agree markedly well with the predictions from the (linear elastic) FE-calculations presented in Section 5. When making these comparisons, note that all presented results there are normalized to be valid for the current clamping ratio r_c, regardless of actual load τ.

7 Conclusions and Discussion

It has here been demonstrated that clamping and subsequent loading of an Ioisipescu shear specimen involves effects which hitherto have not received too much attention. These issues include appropriate levels of such clamping, additional stresses due to this clamping, and risk of premature failure due to the high combined stress levels upon shear loading. Further issues are inevitably high contact pressures at two locations (sometimes referred to as 'inner loading points'), loss of contact on the opposite face of those locations, and quite high tensile stresses in the region where this separation occurs.

It was found that generally a clamping ratio of $r \sim 1$ is the most favourable and minimizes peak compressive stresses at the inner loading points, though still about four times higher than the nominal shear load. Highest tensile loads occur on and along the opposite clamping face. Peak levels there are about 1.2 - 1.35 times the nominal shear for reasonable r, and clamping ratios well in excess of $r \sim 3$ are required to lower those stresses substantially. Incidentally, similarly high clamping ratios are required to completely avoid separation in that gripping region, and for more reasonable r contact will be lost over 20-25%.

These findings were here demonstrated using both simple modelling, detailed numerical analyses and subsequently confirmed by experiments using optical full-field strain measurements. Both the phenomena mentioned, their magnitudes, their locations and spatial extensions agree remarkably well with the numerical results.

Even the simple model gives describes these phenomena fairly well and gives quantitative estimates. However, for obvious reasons it cannot reproduce the almost 'point load'-like stress levels at the inner loading points. It should here also be mentioned that remarkable agreement for the contact pressure levels between numeric ($\hat{p} = 4 \cdot \tau$) and experimental observations ($\hat{p} = 3.88 \cdot \tau$) is somewhat coincidental, since they depend on both FE-meshing and strain field filtering and facet sizes. For the highest tensile stresses however, the agreement is similarly good: $\sigma_x = 1.3 \cdot \tau$ is found numerically, and experimentally it is about $\sigma_x = 1.17 \cdot \tau$, both in the same region. Finally, both the onset of, and the progress and extent of separation also agreed very well among numerical and experimental observations.

Additionally, it was shown that in spite of the many non-linear effects in place, numerical results may be interpreted and scaled to be valid for a quite wide range of loads and materials, and the inaccuracies introduced thereby are minor, and much smaller than other uncertainties and scatter in a real experiment.

Acknowledgements

The authors are indebted to Mr. B. Möllerberg for manufacturing the fixture and specimens, the Knut and Alice Wallenberg foundation for financing the DSP-equipment, and for faculty funding from KTH.

References

[1] Walrath D.E. and Adams D.F., 'The Iosipescu shear test as applied to composite materials'. *Experimental Mechanics*, Vol. 1**2**, pp 131–138, 1990

[2] 'Standard method for shear properties of composite materials by the v-notched beam method', ASTM Designation: D 5379/D 5379M-93, 1993

[3] Neumeister J.M. and Melin L.N. ´A modified Iosipescu shear test for anisotropic composite panels´, SME: *Proc. ICCM 14*, San Diego, USA, 2003

[4] Suo Z., Bao G., Fan B. and Wang T.C. 'Orthotropy rescaling and implications for fracture in composites'. *Int. J. Solids Struct*., Vol. **28**, pp 235–248, 1991

[5] Melin L.N. and Neumeister J.M. ´Sensitivity to specimen imperfections of the Iosipescu shear test for composite laminates´, SME: *Proceedings, ICCM 16*, Kyoto, Japan, 2007

[6] Melin L.N. and Neumeister J.M. 'Measuring constitutive shear behavior of orthotropic composites and evaluation of the modified Ioisipescu test', *Comp. Struct.* Vol. 76, pp 106–115, 2006

[7] Melin L.N. and Neumeister J.M. 'The influence of specimen clamping and specimen imperfections on the Ioisipescu shear test performance' Paper C in Licentiate Thesis, KTH – Solid Mechanics no 99, 2006. To be submitted.